JACS
JOURNAL OF THE AMERICAN CHEMICAL SOCIETY
Article
Cite This: J. Am. Chem. Soc. 2019, 141, 14443−14450
pubs.acs.org/JACS

Robust Corrole-Based Metal−Organic Frameworks with Rare 9-Connected Zr/Hf-Oxo Clusters

Yanming Zhao,[†,‡,§] Shibo Qi,[∥] Zheng Niu,[‡] Yunlei Peng,[⊥] Chuan Shan,[‡] Gaurav Verma,[‡] Lukasz Wojtas,[‡] Zhenjie Zhang,[⊥] Bao Zhang,*[,†] Yaqing Feng,[†,§] Yu-Sheng Chen,[#] and Shengqian Ma*[,‡]

[†]School of Chemical Engineering and Technology, Tianjin University, Tianjin 300350, People's Republic of China
[‡]Department of Chemistry, University of South Florida, Tampa, Florida 33620, United States
[§]Collaborative Innovation Center of Chemical Science and Engineering, Tianjin 300072, People's Republic of China
[∥]School of Chemistry and Chemical Engineering, Tianjin Polytechnic University, Tianjin 300387, People's Republic of China
[⊥]College of Chemistry, Nankai University, Tianjin 300071, People's Republic of China
[#]ChemMatCARS, Center for Advanced Radiation Sources, The University of Chicago, 9700 South Cass Avenue, Argonne, Illinois 60439, United States

Supporting Information

ABSTRACT: The corrole unit from the porphyrinoid family represents one of the most important ligands in the field of coordination chemistry, which creates a unique environment allowing for the observation of unusual electronic states of bound metal cations and has shown great promise in various applications. Nevertheless, studies that directly and systematically introduce these motifs in porous crystalline materials for targeting further functionalizations are still lacking. Herein, we report for the first time the construction of two robust corrole-based metal−organic frameworks (MOFs), $M_6(\mu_3\text{-}O)_4(\mu_3\text{-}OH)_4(OH)_3(H_2O)_3(H_3TCPC)_3$ (M = Zr for **Corrole-MOF-1** and M = Hf for **Corrole-MOF-2**, H_3TCPC = 5,10,15-tris(*p*-carboxylphenyl)corrole), which are assembled by a custom-designed C_{2v}-symmetric corrolic tricarboxylate ligand and the unprecedented D_{3d}-symmetric 9-connected Zr_6/Hf_6 clusters. The resultant frameworks feature a rare (3,9)-connected **gfy** net and exhibit high chemical stability in aqueous solutions within a wide range of pH values. Furthermore, we successfully prepared the cationic **Corrole-MOF-1(Fe)** from the iron corrole ligand, which can serve as an efficient heterogeneous catalyst for [4 + 2] hetero-Diels−Alder reactions between unactivated aldehydes and a simple diene, outperforming both the homogeneous counterpart and the porphyrinic MOF counterpart.

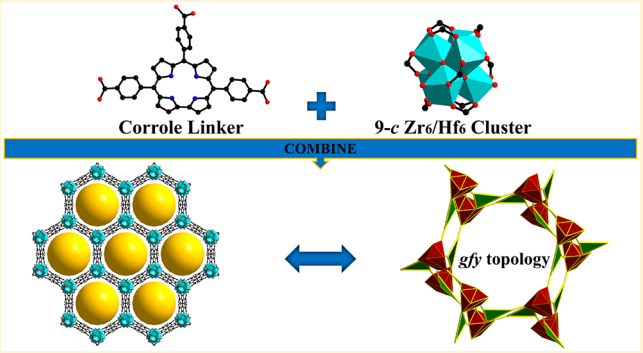

INTRODUCTION

Metal−organic frameworks (MOFs), an emerging class of inorganic−organic hybrid crystalline materials, have evoked great interest due to their high porosity/internal surface areas, structural diversity, and chemical tailorability.[1,2] They have attractive potential in various applications ranging from gas storage/separation[3,4] to proton conduction,[5] biomedicine,[6] and catalysis,[7] to name only a few. Moreover, the tunable nature of MOFs furnishes a prominent advantage over other porous materials in that their further functionalizations can be readily realized by postsynthetic modification toward linkers and/or metal clusters,[8,9] construction of MOF composites by encapsulating active materials such as enzymes,[10,11] metal nanoparticles,[12,13] and organometallic species[14] into the frameworks, or inclusion of functional ligands such as metal complexes as the building units,[15] among which the direct introduction of new promising organic linkers represents one of the most straightforward yet effective methods to target functional MOFs.

Porphyrinoid macrocyclic complexes that can be fine-tuned for specific purposes play important roles in many chemical and biological processes.[16] Among these compounds, corroles pertaining to contracted porphyrin analogues, which hold the 18-π-conjugated structure bearing a direct pyrrole−pyrrole link, have received growing attention because of their unusual photophysical properties and electronic states of bound metal cations as well as the powerful capability of stabilizing high-valent transition metals.[17] These features have made them exhibit distinct advantages over other compounds, especially

Received: July 18, 2019
Published: August 21, 2019

DOI: 10.1021/jacs.9b07700
J. Am. Chem. Soc. 2019, 141, 14443−14450

when they are metallized for use as catalysts, whose utilizations are highlighted in the potent catalase-like activity for decomposing reactive oxygen/nitrogen species,[18,19] the ability to enable both O_2 activation and O−O bond formation reactions,[20] possession of efficient Lewis acid catalytic performance,[21] etc. However, despite the success of developing metallocorroles in applications of homogeneous catalysis, it still encounters some limitations: poor recyclability and stability in solutions lead to a decreased catalyst lifetime,[22] while the large π-conjugated system of corrole complexes prompts the deactivation of the catalyst via intermolecular pathways.[23,24] Such limitations can be overcome via heterogenization of corrole-induced homogeneous catalysis; however, this has barely been achieved.[25]

The tremendous development of MOFs suggests a promising route to resolve the aforementioned issues via incorporation of corrole moieties into an MOF framework, which can couple the interesting properties of corroles and the superiority of MOF structures to afford efficient heterogeneous catalysis. Nevertheless, to the best of our knowledge, to date there have been no reports of corrole-based MOFs, likely due to challenges in structural design and control, in which the unusual approximately T-shaped geometry of corrole ligands impedes the construction of an MOF structure, in contrast to most traditional cases where the high symmetry-guided design is expected to result in the anticipated topology.[1,15a]

In this context, Zr/Hf-oxo clusters as secondary building units (SBUs) are of particular interest in targeting desired MOFs, because of the variation of their connecting numbers and symmetry that could provide many topological possibilities to form different frameworks.[26] For instance, the connectivity of Zr_6 nodes can be tuned to be 4-, 6-, 8-, 10-, or 12-connected (Scheme 1) by ditopic, tritopic, tetratopic, or hexatopic linkers,

Scheme 1. Connectivity of Zr_6 Clusters[a]

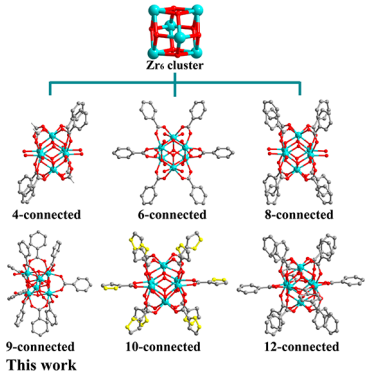

[a]The connectivity refers to the number of carboxylate groups from organic linkers in the extended framework coordinated to the Zr_6 cluster (white, hydrogen; gray, carbon; red, oxygen; yellow, nitrogen; aqua, zirconium).

which offers a formidable means to modulate the degree of freedom at the intersections between the metal nodes and organic linkers.[27,28] Especially, the systematically studied porphyrin-based Zr-MOFs give different structures that contain clusters with the aforementioned connectivities with the exception of the 4- and 10-connected nodes,[26] wherein a combination of the identical porphyrin ligands and 8-connected Zr_6 clusters can assemble into a variety of network topologies including **csq** (PCN-222),[23] **sqc** (PCN-225),[29] and **scu** (NU-902)[30] through the adjustment of synthetic conditions. These studies prompt us to explore the construction of corrole-based Zr-MOFs, and we anticipate their structures will most likely differ substantially from those reported given the geometrical uniqueness of the corrole linker (Figure 1a), which could direct the in situ formation of some new SBUs.

Herein, for the first time, we report two stable corrole-based MOFs, **Corrole-MOF-1** and **-2**, which are constructed from the custom-designed C_{2v}-symmetric tridentate corrole ligand H_3TCPC (5,10,15-tris(*p*-carboxylphenyl)corrole) and the unprecedented D_{3d}-symmetric 9-connected Zr_6/Hf_6 clusters (Scheme 1), respectively, featuring a rare (3,9)-connected **gfy** network (Figure 1c). Both Corrole-MOFs exhibit uniform one-dimensional (1D) hexagonal open channels of 23.4 Å. **Corrole-MOF-1(Fe)** has also been successfully prepared from the iron corrole ligand FeTCPCCl and the Zr_6 cluster, which can efficiently catalyze hetero-Diels−Alder (HDA) reactions between unactivated aldehydes and a simple diene,[31] outperforming both the homogeneous counterpart and the porphyrinic MOF counterpart.

EXPERIMENTAL SECTION

General Information. The commercial chemicals were used as purchased unless otherwise mentioned. The H_3TCPC and FeTCPCCl ligands were prepared according to procedures described in Section 1 in the Supporting Information.

Instrumentation. Powder X-ray diffraction (PXRD) data were collected on a Bruker AXS D8 Advance A25 Powder X-ray diffractometer (40 kV, 40 mA) using Cu Kα (λ = 1.5406 Å) radiation. Gas sorption isotherm measurements were carried out on a Micromeritics ASAP 2020 instrument with different temperatures. N_2 isotherms were performed at 77 K, with the temperature held constant using a liquid N_2 bath. Fourier transform infrared spectra (FTIR) were recorded on a Nicolet Impact 410 FTIR spectrometer. Thermogravimetric analyses (TGA) were carried out on a Q50 thermogravimetric analyzer under a nitrogen atmosphere. Elemental analyses were performed on a PerkinElmer series II CHNS analyzer 2400. Nuclear magnetic resonance (NMR) data were recorded on a Bruker Avance-400 (400 MHz) spectrometer. MALDI-TOF-MS was obtained with a Bruker Autoflex TOF/TOF III instrument. UV−vis absorption spectra were conducted on a JASCO Model V-670 spectrometer. Scanning electron microscopy (SEM) images and energy dispersive spectrometer (EDS) analyses were performed on a Hitachi SU 8000. All of the Corrole-MOFs were activated by supercritical CO_2 performed on a Tousimis Samdri PVT-30 critical point dryer.

Synthesis of Corrole-MOF-1. In a 5 mL glass vial, $ZrCl_4$ (0.054 mmol, 3.0 equiv), H_3TCPC (0.018 mmol, 1.0 equiv), and benzoic acid (1.8 mmol, 100 equiv) were dissolved in *N*,*N*-dimethylformamide (DMF, 1.0 mL) via sonication (30 min). The green solution was heated at 120 °C for 72 h in an oven. After the mixture was cooled to room temperature, hexagonal purple crystals were harvested by filtration (yield 87%). Anal. Calcd: C, 52.77; H, 2.20; N, 6.16. Found: C, 52.03; H, 2.36; N, 6.01.

Synthesis of Corrole-MOF-2. In a 5 mL glass vial, $HfCl_4$ (0.054 mmol, 3.0 equiv), H_3TCPC (0.018 mmol, 1.0 equiv), and benzoic acid (1.8 mmol, 100 equiv) were dissolved in DMF (1.0 mL) via sonication (30 min). The green solution was heated at 120 °C for 72 h in an oven. After the mixture was cooled to room temperature, hexagonal purple crystals were harvested by filtration (yield 73%). Anal. Calcd (%): C, 44.28; H, 1.85; N, 5.17. Found (%): C, 44.73; H, 1.92; N, 4.98.

Synthesis of Corrole-MOF-1(Fe). In a 5 mL glass vial, $ZrCl_4$ (0.054 mmol, 3.0 equiv), FeTCPCCl (0.018 mmol, 1.0 equiv), and acetic acid (7.87 mmol, 437 equiv) were dissolved in DMF (1.0 mL) via sonication (30 min). The brown solution was heated at 120 °C for

DOI: 10.1021/jacs.9b07700
J. Am. Chem. Soc. 2019, 141, 14443−14450

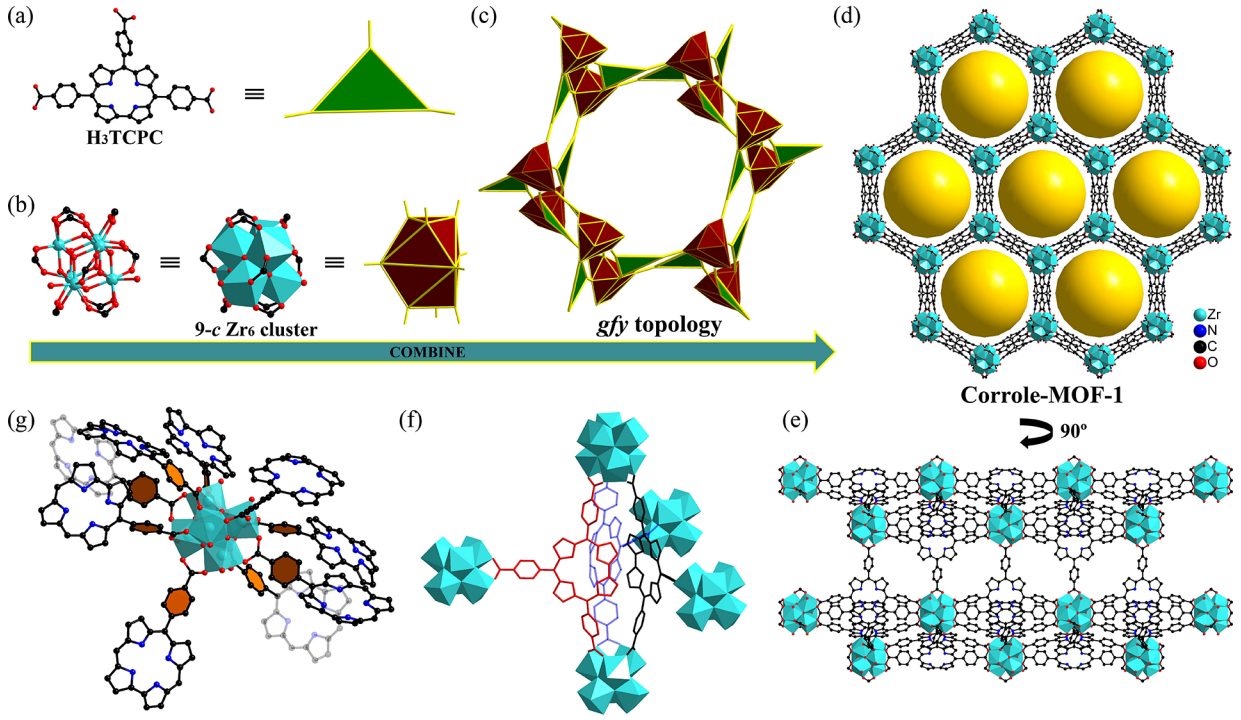

Figure 1. Crystal structure, structural components, and underlying network topology of **Corrole-MOF-1** after removal of disorder: (a) tricarboxylic corrolic linker, H_3TCPC; (b) D_{3d}-symmetric 9-connected Zr_6 cluster; (c) schematic representation of the (3,9)-connected net for **Corrole-MOF-1** framework; (d, e) View of **Corrole-MOF-1** along the *c* and *a* axes, respectively, with uniform 1D open channels; (f, g) magnified parts in the structure displaying the connectivity between corrole ligands and Zr_6 clusters. The Zr, C, O, and N atoms are shown as aqua, black, red, and blue spheres, respectively. H atoms are omitted for clarity.

72 h in an oven. After the mixture was cooled to room temperature, brown powders were obtained for characterization (yield 84%). Anal. Calcd (%): C, 51.10; H, 2.02; N, 5.96. Found (%): C, 51.46; H, 2.13; N, 5.77. Purple hexagonal single crystals of **Corrole-MOF-1 and -2** with suitable sizes for single-crystal X-ray diffraction have been obtained in our experiments. **Corrole-MOF-1(Fe)** was confirmed by a powder X-ray diffraction pattern.

Single-Crystal X-ray Crystallography. The X-ray diffraction data for **Corrole-MOF-1** were measured on a Bruker D8 Venture PHOTON II CPAD system equipped with a Cu Kα INCOATEC ImuS microfocus source (λ = 1.54178 Å). The X-ray diffraction data for **Corrole-MOF-2** were collected using synchrotron radiation (λ = 0.41328 Å) at the Advanced Photon Source, Beamline 15-ID-B of ChemMatCARS in Argonne National Laboratory, Argonne, IL. Indexing was performed using APEX3 (Difference Vectors method). Data integration and reduction were performed using SaintPlus. Absorption correction was performed by a multiscan method implemented in SADABS. Space groups were determined using XPREP implemented in APEX3. Structures were solved using SHELXT and refined using SHELXL-2018 (full-matrix least-squares on F^2) through the OLEX2 interface program.

Corrole-MOF-1 and **-2** crystals (constructed from Zr_6 and Hf_6 clusters, respectively) are isostructural. In both cases diffraction frames contain diffuse streaks/lines and reflections are visibly clustered into groups. Both structures were modeled in the highest symmetry ($P6_3/mmc$) suggested by data analyses, which is consistent with observed ligand and cluster disorder over two positions. The observed disorder could possibly be due to two possible conformations of the benzoate part perpendicular to the *c* crystallographic direction that would result in two possible orientations of the metal cluster rotated by 60°. Disordered atoms were refined with restraints. The contribution of disordered content in structural voids in both cases was treated as diffuse using the Squeeze procedure implemented in the Platon program. Crystallographic data and structural refinements for **Corrole-MOF-1** and **-2** are summarized in Table S1 in the Supporting Information. The CIF files can be obtained free of charge from the Cambridge Crystallographic Data Centre via www.ccdc.cam.ac.uk/data_request/cif (CCDC 1939968 for **Corrole-MOF-1**, CCDC 1939478 for **Corrole-MOF-2**).

Sample Activation and Gas Sorption Measurement. Before a gas sorption experiment, as-synthesized Corrole-MOF samples (~60 mg) were washed three times with DMF and three times with methanol, followed by soaking in methanol for 72 h to allow solvent exchange. During the solvent exchange process, the methanol was decanted and replaced with fresh solvent for three times every 24 h. After that, the Corrole-MOF powders were isolated by centrifugation. Then, the resulting exchanged frameworks were activated by supercritical CO_2 (detailed procedures are given in Section 6 in the Supporting Information), prior to gas sorption measurement.

Stability Test. For a solvent stability study, small amounts of freshly synthesized **Corrole-MOF-1** (~10 mg) were placed in different vials containing 3 mL of solvent or aqueous solution with a certain pH value. After 24 h, the samples were washed twice with fresh DMF for PXRD measurements or activated by supercritical CO_2 for N_2 adsorption tests.

Catalysis. An oven-dried Schlenk tube was charged with **Corrole-MOF-1(Fe)** (0.02 mmol) and $AgBF_4$ (0.1 mmol) under a dry nitrogen atomosphere in a glovebox. Dry CH_2Cl_2 (2.0 mL) was added by syringe. The mixture was stirred for 3 h at room temperature. Then to the mixture were added aldehyde (1.0 mmol), the diene (4.0 mmol), and dry toluene (6.0 mL) under the nitrogen protection in the glovebox. The tube was sealed and heated to 80 °C. After 24 h, the reactor was cooled to room temperature and depressurized. A ^{1}H NMR analysis in conjugation with column chromatography isolation were employed to determine the conversion. The reaction solution was centrifuged to recover the catalyst for the next cycle. The recovered MOF powders were washed with DMF and methanol and activated by supercritical CO_2. The structural stability of the framework after three recycles was confirmed by PXRD.

DOI: 10.1021/jacs.9b07700
J. Am. Chem. Soc. 2019, 141, 14443−14450

RESULTS AND DISCUSSION

Hexagon-shaped single crystals of **Corrole-MOF-1** and **-2**, $M_6(\mu_3\text{-O})_4(\mu_3\text{-OH})_4(OH)_3(H_2O)_3(H_3TCPC)_3$ (M = Zr for **1** and M = Hf for **2**), were obtained by a solvothermal reaction of $ZrCl_4$ or $HfCl_4$ with H_3TCPC in DMF in the presence of benzoic acid at 120 °C. Similar conditions afforded the polycrystalline **Corrole-MOF-1(Fe)** of $Zr_6(\mu_3\text{-O})_4(\mu_3\text{-OH})_4(OH)_3(H_2O)_3(FeTCPCCl)_3$ with the addition of acetic acid. PXRD patterns suggested that these MOFs have the same framework topology (Figure 2a), and the structure of **Corrole-MOF-1** will be discussed below as a representative.

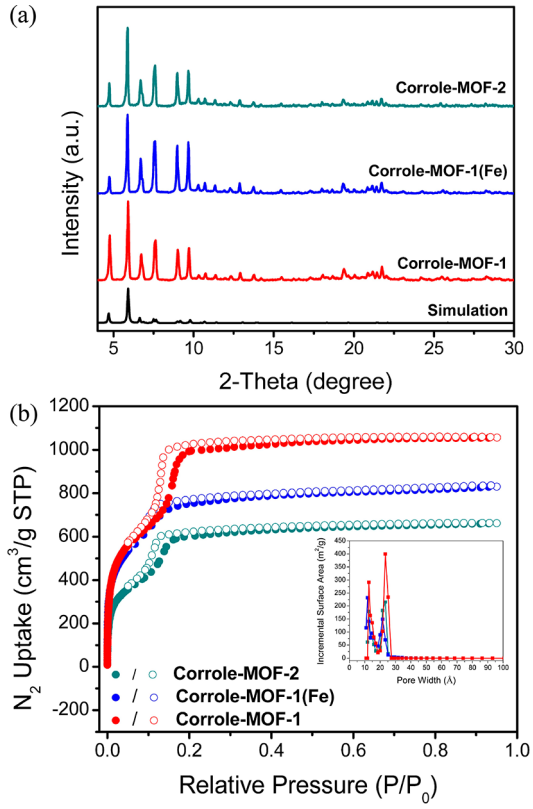

Figure 2. (a) PXRD patterns and (b) N_2 sorption isotherms for **Corrole-MOF-1**, **Corrole-MOF-1(Fe)**, and **Corrole-MOF-2** at 77 K. The inset shows pore size distributions.

Single-crystal X-ray diffraction studies revealed that both **Corrole-MOF-1** and **-2** crystallize in the hexagonal space group $P6_3/mmc$. The structure of **Corrole-MOF-1** involves 9-connected $Zr_6(\mu_3\text{-O})_4(\mu_3\text{-OH})_4(OH)_3(H_2O)_3(COO)_9$ SBUs, which are linked through 3-connected $TCPC^{3-}$ ligands to form a 3D framework containing large hexagonal 1D open channels along the *c* axis (Figure 1d and e). The SBU is composed of six Zr atoms assembled into an octahedral $Zr_6(\mu_3\text{-O})_4(\mu_3\text{-OH})_4$ cluster core where only nine edges are bridged by the carboxylates from $TCPC^{3-}$ linkers, while the remaining six positions are occupied by $\mu_3\text{-}O^{2-}/OH^-$ groups (Figure 1b). In comparison with the well-known 12-*c* Zr_6 cluster,[32] the symmetry of the 9-*c* Zr_6 cluster is reduced from O_h to D_{3d}, which is affected by the approximately T-shaped geometry of H_3TCPC (Figures S5−S7 in the Supporting Information). The solvent-accessible volumes in **Corrole-MOF-1** and **-2** are calculated to be 68.8 and 68.5% respectively, using the PLATON routine.[33] Topologically, the H_3TCPC ligand and Zr_6 cluster can be respectively viewed as 3- and 9-*c* nodes. Thus, the **Corrole-MOF-1** framework is classified as a 3D (3,9)-connected **gfy** net with the point symbol of $(4^{12}\cdot6^{15}\cdot8^9)(4^3)_3$ calculated using the TOPOS program (Figure 1c). There have been very few (3,9)-*c* MOFs reported,[34] and **Corrole-MOF-1** represents the first example of a zirconium MOF with (3,9)-*c* **gfy** topology.

N_2 sorption isotherms were collected at 77 K to evaluate the porosity of Corrole-MOFs (Figure 2b). The typical type IV isotherm of **Corrole-MOF-1** shows a steep increase at P/P_0 = 0.15 with a significant hysteresis loop, characteristic of mesoporous materials. On the basis of the N_2 adsorption data, a Brunauer−Emmett−Teller (BET) surface area of 2545 $m^2\ g^{-1}$ and a total pore volume of 1.63 $cm^3\ g^{-1}$ were calculated for **Corrole-MOF-1** upon activation with acid aqueous solutions (Figure S16 in the Supporting Information). The pore size distribution calculated by density functional theory (DFT) from the N_2 sorption curve indicates that the pores of **Corrole-MOF-1** are predominantly distributed at 12.7 and 23.4 Å, assignable to the microporous channels along the *a* and *b* axes and the mesoporous hexagonal channels along the *c* axis respectively, which are consistent with the crystallographic data when the van der Waals contact is taken into account (Figures 1 and 2b). The BET surface areas of **Corrole-MOF-1(Fe)** and **Corrole-MOF-2** are 2145 and 1662 $m^2\ g^{-1}$, respectively, as estimated from the N_2 sorption isotherms (Figure 2b and Table S2 in the Supporting Information). Thermogravimetric analyses indicated that the Corrole-MOFs are stable up to 350 °C under a nitrogen atmosphere (Figure S11 in the Supporting Information).

Although **Corrole-MOF-1** is built from the low-symmetry ligand and Zr_6 clusters with relatively low connectivity among Zr-MOFs,[26] it still demonstrates excellent chemical stability in various solvents and aqueous solutions of a wide pH range. After treatment under these various conditions, the PXRD patterns of **Corrole-MOF-1** remain intact, suggesting the retention of crystallinity and structural integrity (Figure 3a and Figure S28 in the Supporting Information). To further investigate the stability of **Corrole-MOF-1**, N_2 sorption isotherms were measured after immersing samples in water, boiling water, and pH 2 and 11 aqueous solutions for 24 h. The N_2 uptakes of **Corrole-MOF-1** after different treatments are comparable to that of the pristine sample, indicative of the robustness of the framework under harsh conditions (Figure 3b and Table S3 in the Supporting Information). Such excellent chemical stability of Corrole-MOFs makes them hold promise for many applications.

The employment of Corrole-MOFs as heterogeneous catalysts was examined in the context of investigating the Lewis acid catalytic activity of **Corrole-MOF-1(Fe)** for the [4 + 2] hetero-Diels−Alder (HDA) reaction between unactivated aldehydes and a simple diene. HDA reactions have been viewed as some of the very efficient and atom-economical approaches for the synthesis of dihydropyrans, an important class of ubiquitous motifs in biologically active compounds.[31] In general, HDA reactions between unactivated aldehydes and dienes require strong Brønsted acids or Lewis acids, which limit the substrate choice due to low functional group tolerance.[35] To overcome these drawbacks, a breakthrough using cationic iron macrocycle complexes such as iron(III) porphyrin and iron(IV) corrole as homogeneous catalysts can efficiently catalyze HDA reactions between unreactive aldehydes and dienes under mild reaction conditions.[21a,36]

DOI: 10.1021/jacs.9b07700
J. Am. Chem. Soc. 2019, 141, 14443−14450

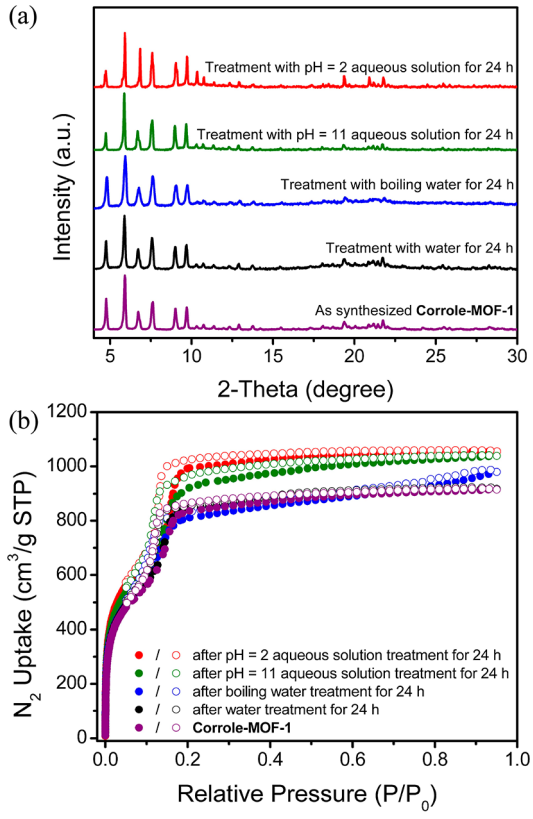

Figure 3. (a) PXRD patterns and (b) N_2 sorption isotherms for **Corrole-MOF-1** at 77 K, showing the framework stability upon treatment with water, boiling water, and aqueous solutions with pH values of 2 and 11.

However, it should be noted that homogeneous corrole-based catalysts normally suffer from poor stability and recyclability.[22] The incorporation of corrole complexes into MOFs for use in heterogeneous systems would offer an effective strategy to improve the catalyst lifetime and to make the catalyst prone to be recoverable. Meanwhile, the deactivation of the catalyst via intermolecular pathways can also be well-restrained, which facilitates the catalytic processes. As expected, the integration of excellent chemical stability, large porosity and surface areas, and high density of catalytically active sites makes **Corrole-MOF-1(Fe)** an excellent heterogeneous catalyst for this reaction.

Notwithstanding, only a trace amount of product **3a** was obtained when **Corrole-MOF-1(Fe)** was used as the catalyst in the reaction of benzaldehyde (**1a**) with 2,3-dimethyl-1,3-butadiene (**2**), probably due to the presence of a strong axially coordinating chloride anion on the catalytic iron center blocking the catalytic process (Table S4, entry 2, in the Supporting Information). To remedy this, the cationic catalyst **[Corrole-MOF-1(Fe)]BF_4** was prepared by treating **Corrole-MOF-1(Fe)** with $AgBF_4$, in order to weaken the coordination strength of the counteranion.[36,37] Encouragingly, the reaction of **1a** with **2** in the presence of **[Corrole-MOF-1(Fe)]BF_4** (2 mol %) in toluene at 80 °C for 24 h afforded dihydropyran **3a** in 96% yield (93% isolated yield) in comparison to only 67% yield in the presence of the homogeneous ester-corrole catalyst Fe(TCMPC)BF_4 (Table 1, entries 1 and 2). The enhanced catalytic activity of **[Corrole-MOF-1(Fe)]BF_4** in comparison with the homogeneous system presumably originates from the high porosity, facilitating mass transport and maximizing the accessibility of catalytic sites. Additionally, the presence of strongly electron withdrawing units including three carboxylate groups attached to the corrole ring and the zirconium clusters could decrease the electron density of iron(IV) in the corrole ligands, which further increases the polarizability of the iron center, thus enhancing the catalytic performance (Figure S30 in the Supporting Information).[37,38] Free base **Corrole-MOF-1** is inactive for the HDA reaction (Table S4, entry 1, in the Supporting Information), meaning there is a minimal

Table 1. [4+2] Hetero-Diels–Alder Reactions of Aldehydes with a Diene[a]

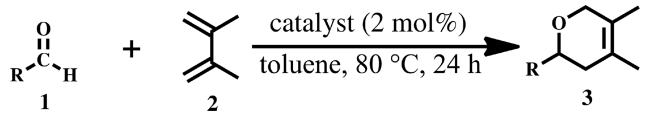

entry	product	catalyst	yield (%)[b]
1	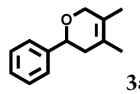 **3a**	**[Corrole-MOF-1(Fe)]BF_4**	93 (96)
2		Fe(TCMPC)BF_4	67[c]
3[d]	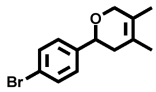 **3b**	**[Corrole-MOF-1(Fe)]BF_4**	92
4		PCN-224(Fe)BF_4	83
5	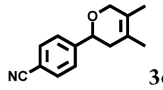 **3c**	**[Corrole-MOF-1(Fe)]BF_4**	87
6	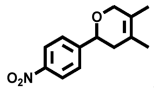 **3d**	**[Corrole-MOF-1(Fe)]BF_4**	81
7	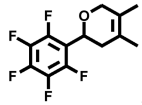 **3e**	**[Corrole-MOF-1(Fe)]BF_4**	73
8	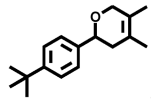 **3f**	**[Corrole-MOF-1(Fe)]BF_4**	77
9	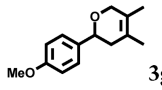 **3g**	**[Corrole-MOF-1(Fe)]BF_4**	94
10	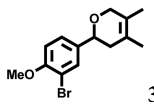 **3h**	**[Corrole-MOF-1(Fe)]BF_4**	89

[a]Reaction conditions: catalyst (2 mol %), aldehyde (1.0 mmol), and diene (4.0 mmol) in 6.0 mL of toluene at 80 °C. [b]Isolated yield (yield in parentheses is calculated by ^{1}H NMR with mesitylene as the internal standard). [c]Yield determined by ^{1}H NMR (homogeneous catalysis). [d]Porphyrinic MOF PCN-224(Fe)BF_4 as the catalyst.

DOI: 10.1021/jacs.9b07700
J. Am. Chem. Soc. 2019, 141, 14443–14450

contribution from zirconium clusters to the catalytic activity of [**Corrole-MOF-1(Fe)**]BF_4.

To further investigate the scope and limitations of corrole MOF-catalyzed HDA reactions, benzaldehydes bearing different electron-withdrawing and/or electron-donating substituents were tested. The dihydropyran products all formed in excellent yields in comparison to homogeneous systems (Table 1 and Table S4 in the Supporting Information). It was found that both electronic and steric effects in the aldehydes could influence the reaction, in which strong electron-withdrawing substituents led to lower yield in comparison to electron-donating groups. Particularly, the lowest yield was resulted for the reaction of pentafluorobenzaldehyde (**1e**), while the reaction of *p-tert*-butylbenzaldehyde (**1f**) with **2** produced **3f** in a moderate 77% yield, which is likely attributed to the steric effect of the large-sized *tert*-butyl substituent (Table 1, entries 7 and 8). In comparison with [**Corrole-MOF-1(Fe)**]BF_4, the porphyrinic MOF PCN-224(Fe)BF_4 catalyzed HDA reactions of aldehydes (**1b,c,g**) with **2** resulted in the lower yields of the desired dihydropyran products **3** (Table 1, entries 3−5 and 9, and Table S4, entries 12 and 21, in the Supporting Information).[28b] The higher reactivity for [**Corrole-MOF-1(Fe)**]BF_4 is probably due to the higher polarization and the increased Lewis acidity of the center metal iron(IV) in the corrole ligands,[21a,37] which has a higher oxidation state in comparison to that of iron(III) in the porphyrin ligands. Owing to the high stability of Corrole-MOFs, [**Corrole-MOF-1(Fe)**]BF_4 can be recycled and maintain high catalytic activity after three cycles, with retention of structural integrity as suggested by PXRD patterns (Table S4, entry 24, and Figure S32 in the Supporting Information).

CONCLUSION

In conclusion, zirconium- and hafnium-corrole frameworks, **Corrole-MOF-1** and **-2**, have been constructed for the first time employing a custom-designed corrole ligand and the unprecedented 9-connected Zr_6/Hf_6 clusters. The resultant Corrole-MOFs possess a very rare (3,9)-*c* **gfy** network and feature 1D hexagonal mesoporous open channels as well as demonstrate high chemical stability and framework robustness. The exploration of corrole-based MOFs as heterogeneous catalysts has been demonstrated in the context of [**Corrole-MOF-1(Fe)**]BF_4-catalyzed hetero-Diels−Alder reactions of unactivated aldehydes with a simple diene, which exhibits excellent performance surpassing both the homogeneous counterpart and porphyrinic MOF counterpart. Our studies not only enrich the family of MOFs but also pave the way for the development of corrole-functionalized porous materials in a broader range of applications.

ASSOCIATED CONTENT

Supporting Information

The Supporting Information is available free of charge on the ACS Publications website at DOI: 10.1021/jacs.9b07700.

Ligand synthesis and characterization, additional structure figures, characterization of Corrole-MOFs, additional sorption isothermal analysis and BET statistics, catalytic studies of hetero-Diels−Alder reaction using Corrole-MOF-1(Fe), and comparison with other catalysts (PDF)

X-ray crystallographic data for **Corrole-MOF-1** (CIF)

X-ray crystallographic data for **Corrole-MOF-2** (CIF)

AUTHOR INFORMATION

Corresponding Authors

*E-mail for B.Z.: baozhang@tju.edu.cn.

*E-mail for S.M.: sqma@usf.edu.

ORCID

Zhenjie Zhang: 0000-0003-2053-3771

Bao Zhang: 0000-0003-4846-0594

Shengqian Ma: 0000-0002-1897-7069

Notes

The authors declare no competing financial interest.

ACKNOWLEDGMENTS

The authors acknowledge the China International Science and Technology Project (NO. 2016YFE0114900), National Natural Science Foundation of China (NO. 21761132007), China Scholarship Council (CSC) (NO. 201706250095), United States National Science Foundation (DMR-1352065), and the University of South Florida for financial support of this work.

REFERENCES

(1) Furukawa, H.; Cordova, K. E.; O'Keeffe, M.; Yaghi, O. M. The Chemistry and Applications of Metal-Organic Frameworks. *Science* **2013**, *341*, 1230444.

(2) (a) Kirchon, A.; Feng, L.; Drake, H. F.; Joseph, E. A.; Zhou, H.-C. From fundamentals to applications: a toolbox for robust and multifunctional MOF materials. *Chem. Soc. Rev.* **2018**, *47*, 8611. (b) Li, B.; Chrzanowski, M.; Zhang, Y.; Ma, S. Applications of Metal-Organic Frameworks Featuring multi-Functional Sites. *Coord. Chem. Rev.* **2016**, *307*, 106.

(3) (a) Ma, S.; Zhou, H.-C. Gas Storage in Porous Metal-Organic Frameworks for Clean Energy Applications. *Chem. Commun.* **2010**, *46*, 44. (b) He, Y.; Chen, F.; Li, B.; Qian, G.; Zhou, W.; Chen, B. Porous Metal-Organic Frameworks for Fuel Storage. *Coord. Chem. Rev.* **2018**, *373*, 167.

(4) (a) Lin, R. B.; Xiang, S. C.; Xing, H. B.; Zhou, W.; Chen, B. L. Exploration of Porous Metal-Organic Frameworks for Gas Separation and Purification. *Coord. Chem. Rev.* **2019**, *378*, 87. (b) Niu, Z.; Cui, X.; Pham, T.; Lan, P. C.; Xing, H.; Forrest, K. A.; Wojtas, L.; Space, B.; Ma, S. A Metal-Organic Framework Based Methane Nano-trap for the Capture of Coal-Mine Methane. *Angew. Chem., Int. Ed.* **2019**, *58*, 10138.

(5) Meng, X.; Wang, H.-N.; Song, S.-Y.; Zhang, H.-J. Proton-Conducting Crystalline Porous Materials. *Chem. Soc. Rev.* **2017**, *46*, 464.

(6) Lu, K.; Aung, T.; Guo, N.; Weichselbaum, R.; Lin, W. Nanoscale Metal-Organic Frameworks for Therapeutic, Imaging, and Sensing Applications. *Adv. Mater.* **2018**, *30*, 1707634.

(7) (a) Chughtai, A. H.; Ahmad, N.; Younus, H. A.; Laypkovc, A.; Verpoort, F. Metal-Organic Frameworks: Versatile Heterogeneous Catalysts for Efficient Catalytic Organic Transformations. *Chem. Soc. Rev.* **2015**, *44*, 6804. (b) Jiao, L.; Wang, Y.; Jiang, H. L.; Xu, Q. Metal-Organic Frameworks as Platforms for Catalytic Applications. *Adv. Mater.* **2018**, *30*, 1703663. (c) Wang, X.-K.; Liu, J.; Zhang, L.; Dong, L.-Z.; Li, S.-L.; Kan, Y.-H.; Li, D.-S.; Lan, Y.-Q. Monometallic Catalytic Models Hosted in Stable Metal-Organic Frameworks for Tunable CO_2 Photoreduction. *ACS Catal.* **2019**, *9*, 1726.

(8) (a) Cohen, S. M. The Postsynthetic Renaissance in Porous Solids. *J. Am. Chem. Soc.* **2017**, *139*, 2855. (b) Yin, Z.; Wan, S.; Yang, J.; Kurmoo, M.; Zeng, M.-H. Recent Advances in Post-Synthetic Modification of Metal-Organic Frameworks: New types and Tandem Reactions. *Coord. Chem. Rev.* **2019**, *378*, 500. (c) Gao, W.-Y.; Wu, H.; Leng, K.; Sun, Y.; Ma, S. Inserting CO_2 into Aryl C-H Bond of Metal-Organic Framework: CO_2 Utilization for Direct Heterogeneous C-H Activation. *Angew. Chem., Int. Ed.* **2016**, *55*, 5472.

(9) (a) Niu, Z.; Gunatilleke, W. D. C. B.; Sun, Q.; Lan, P. C.; Perman, J.; Ma, J.-G.; Cheng, Y.; Aguila, B.; Ma, S. Metal-Organic Framework Anchored with a Lewis Pair as a New Paradigm for Catalysis. *Chem.* **2018**, *4*, 2587. (b) Niu, Z.; Zhang, W.; Lan, P. C.; Aguila, B.; Ma, S. Promoting Frustrated Lewis Pair for Heterogeneous Chemoselective Hydrogenation via Tailored Pore Environment within Metal-Organic Framework. *Angew. Chem., Int. Ed.* **2019**, *58*, 7420.

(10) (a) Lykourinou, V.; Chen, Y.; Wang, X.-S.; Meng, L.; Hoang, T.; Ming, L.-J.; Musselman, R. L.; Ma, S. Immobilization of MP-11 into a Mesoporous Metal-Organic Framework, MP-11@mesoMOF: A New Platform for Enzymatic Catalysis. *J. Am. Chem. Soc.* **2011**, *133*, 10382. (b) Chen, Y.; Lykourinou, V.; Vetromile, C.; Hoang, T.; Ming, L.-J.; Larsen, R. W.; Ma, S. How Can Proteins Enter the Interior of a MOF? Investigation of Cytochrome *c* Translocation into a MOF Consisting of Mesoporous Cages with Microporous Windows. *J. Am. Chem. Soc.* **2012**, *134*, 13188. (c) Pan, Y.; Li, H.; Farmakes, J.; Xiao, F.; Chen, B.; Ma, S.; Yang, Z. How do Enzymes Orient when Trapped on Metal-Organic Framework (MOF) Surfaces. *J. Am. Chem. Soc.* **2018**, *140*, 16032.

(11) (a) Lian, X.; Fang, Y.; Joseph, E.; Wang, Q.; Li, J.; Banerjee, S.; Lollar, C.; Wang, X.; Zhou, H.-C. Enzyme−MOF (metal-organic framework) composites. *Chem. Soc. Rev.* **2017**, *46*, 3386. (b) An, H.; Li, M.; Gao, J.; Zhang, Z.; Ma, S.; Chen, Y. Incorporation of Biomolecules in Metal-Organic Frameworks for Advanced Applications. *Coord. Chem. Rev.* **2019**, *384*, 90.

(12) Yang, Q.; Xu, Q.; Jiang, H.-L. Metal-organic frameworks meet metal nanoparticles: synergistic effect for enhanced catalysis. *Chem. Soc. Rev.* **2017**, *46*, 4774.

(13) Liu, Y.; Liu, Z.; Huang, D.; Cheng, M.; Zeng, G.; Lai, C.; Zhang, C.; Zhou, C.; Wang, W.; Jiang, D.; Wang, H.; Shao, B. Metal or metal-containing nanoparticle@MOF nanocomposites as a promising type of photocatalyst. *Coord. Chem. Rev.* **2019**, *388*, 63.

(14) (a) Han, Q.; He, C.; Zhao, M.; Qi, B.; Niu, J.; Duan, C. Engineering Chiral Polyoxometalate Hybrid Metal-Organic Frameworks for Asymmetric Dihydroxylation of Olefins. *J. Am. Chem. Soc.* **2013**, *135*, 10186. (b) Grigoropoulos, A.; Whitehead, G. F. S.; Perret, N.; Katsoulidis, A. P.; Chadwick, F. M.; Davies, R. P.; Haynes, A.; Brammer, L.; Weller, A. S.; Xiao, J.; Rosseinsky, M. J. Encapsulation of an organometallic cationic catalyst by direct exchange into an anionic MOF. *Chem. Sci.* **2016**, *7*, 2037. (c) Kong, X.-J.; Lin, Z.; Zhang, Z.-M.; Zhang, T.; Lin, W. Hierarchical Integration of Photosensitizing Metal-Organic Frameworks and Nickel-Containing Polyoxometalates for Efficient Visible-Light-Driven Hydrogen Evolution. *Angew. Chem., Int. Ed.* **2016**, *55*, 6411. (d) Paille, G.; Gomez-Mingot, M.; Roch-Marchal, C.; Lassalle-Kaiser, B.; Mialane, P.; Fontecave, M.; Mellot-Draznieks, C.; Dolbecq, A. A Fully Noble Metal-Free Photosystem Based on Cobalt-Polyoxometalates Immobilized in a Porphyrinic Metal-Organic Framework for Water Oxidation. *J. Am. Chem. Soc.* **2018**, *140*, 3613.

(15) (a) Lu, W.; Wei, Z.; Gu, Z.-Y.; Liu, T.-F.; Park, J.; Park, J.; Tian, J.; Zhang, M.; Zhang, Q.; Gentle III, T.; Bosch, M.; Zhou, H.-C. Tuning the structure and function of metal-organic frameworks via linker design. *Chem. Soc. Rev.* **2014**, *43*, 5561. (b) Gao, W.-Y.; Chrzanowski, M.; Ma, S. Metal-metalloporphyrin frameworks: a resurging class of functional materials. *Chem. Soc. Rev.* **2014**, *43*, 5841.

(16) (a) Baglia, R. A.; Zaragoza, J. P. T.; Goldberg, D. P. Biomimetic Reactivity of Oxygen-Derived Manganese and Iron Porphyrinoid Complexes. *Chem. Rev.* **2017**, *117*, 13320. (b) Matano, Y. Synthesis of Aza-, Oxa-, and Thiaporphyrins and Related Compounds. *Chem. Rev.* **2017**, *117*, 3138. (c) Sarma, T.; Panda, P. K. Annulated Isomeric, Expanded, and Contracted Porphyrins. *Chem. Rev.* **2017**, *117*, 2785.

(17) (a) Thomas, K. E.; Alemayehu, A. B.; Conradie, J.; Beavers, C. M.; Ghosh, A. The Structural Chemistry of Metallocorroles: Combined Xray Crystallography and Quantum Chemistry Studies Afford Unique Insights. *Acc. Chem. Res.* **2012**, *45*, 1203. (b) Ghosh, A. Electronic Structure of Corrole Derivatives: Insights from Molecular Structures, Spectroscopy, Electrochemistry, and Quantum Chemical Calculations. *Chem. Rev.* **2017**, *117*, 3798. (c) Barata, J. F. B.; Neves, M. G. P. M. S.; Faustino, M. A. F.; Tomé, A. C.; Cavaleiro, J. A. S. Strategies for Corrole Functionalization. *Chem. Rev.* **2017**, *117*, 3192. (d) Aviv, I.; Gross, Z. Corrole-based applications. *Chem. Commun.* **2007**, 1987. (e) Mahammed, A.; Gross, Z. Corroles as triplet photosensitizers. *Coord. Chem. Rev.* **2019**, *379*, 121. (f) Teo, R. D.; Hwang, J. Y.; Termini, J.; Gross, Z.; Gray, H. B. Fighting Cancer with Corroles. *Chem. Rev.* **2017**, *117*, 2711.

(18) Mahammed, A.; Gross, Z. Highly efficient catalase activity of metallocorroles. *Chem. Commun.* **2010**, *46*, 7040.

(19) Haber, A.; Mahammed, A.; Fuhrman, B.; Volkova, N.; Coleman, R.; Hayek, T.; Aviram, M.; Gross, Z. Amphiphilic/Bipolar Metallocorroles That Catalyze the Decomposition of Reactive Oxygen and Nitrogen Species, Rescue Lipoproteins from Oxidative Damage, and Attenuate Atherosclerosis in Mice. *Angew. Chem., Int. Ed.* **2008**, *47*, 7896.

(20) Guo, M.; Lee, Y.-M.; Gupta, R.; Seo, M. S.; Ohta, T.; Wang, H.-H.; Liu, H.-Y.; Dhuri, S. N.; Sarangi, R.; Fukuzumi, S.; Nam, W. Dioxygen Activation and O-O Bond Formation Reactions by Manganese Corroles. *J. Am. Chem. Soc.* **2017**, *139*, 15858.

(21) (a) Kuwano, T.; Kurahashi, T.; Matsubara, S. Iron Corrole-catalyzed [4 + 2] Cycloaddition of Dienes and Aldehydes. *Chem. Lett.* **2013**, *42*, 1241. (b) Tiffner, M.; Gonglach, S.; Haas, M.; Schöfberger, W.; Waser, M. CO_2 Fixation with Epoxides under Mild Conditions with a Cooperative Metal Corrole/Quaternary Ammonium Salt Catalyst System. *Chem. - Asian J.* **2017**, *12*, 1048.

(22) Senge, M. O.; Sergeeva, N. N. Metamorphosis of Tetrapyrrole Macrocycles. *Angew. Chem., Int. Ed.* **2006**, *45*, 7492.

(23) Feng, D.; Gu, Z.-Y.; Li, J.-R.; Jiang, H.-L.; Wei, Z.; Zhou, H.-C. Zirconium-Metalloporphyrin PCN-222: Mesoporous Metal-Organic Frameworks with Ultrahigh Stability as Biomimetic Catalysts. *Angew. Chem., Int. Ed.* **2012**, *51*, 10307.

(24) Wang, K.; Feng, D.; Liu, T.-F.; Su, J.; Yuan, S.; Chen, Y.-P.; Bosch, M.; Zou, X.; Zhou, H.-C. A Series of Highly Stable Mesoporous Metalloporphyrin Fe-MOFs. *J. Am. Chem. Soc.* **2014**, *136*, 13983.

(25) Friedman, A.; Landau, L.; Gonen, S.; Gross, Z.; Elbaz, L. Efficient Bio-Inspired Oxygen Reduction Electrocatalysis with Electropolymerized Cobalt Corroles. *ACS Catal.* **2018**, *8*, 5024.

(26) Yuan, S.; Feng, L.; Wang, K.; Pang, J.; Bosch, M.; Lollar, C.; Sun, Y.; Qin, J.; Yang, X.; Zhang, P.; Wang, Q.; Zou, L.; Zhang, Y.; Zhang, L.; Fang, Y.; Li, J.; Zhou, H.-C. Stable Metal-Organic Frameworks: Design, Synthesis, and Applications. *Adv. Mater.* **2018**, *30*, 1704303.

(27) Chen, Z.; Hanna, S. L.; Redfern, L. R.; Alezi, D.; Islamoglu, T.; Farha, O. K. Reticular chemistry in the rational synthesis of functional zirconium cluster-based MOFs. *Coord. Chem. Rev.* **2019**, *386*, 32.

(28) (a) Zhang, Y.; Zhang, X.; Lyu, J.; Otake, K.-I.; Wang, X.; Redfern, L. R.; Malliakas, C. D.; Li, Z.; Islamoglu, T.; Wang, B.; Farha, O. K. A Flexible Metal-Organic Framework with 4-Connected Zr_6 Nodes. *J. Am. Chem. Soc.* **2018**, *140*, 11179. (b) Feng, D.; Chung, W.-C.; Wei, Z.; Gu, Z.-Y.; Jiang, H.-L.; Chen, Y.-P.; Darensbourg, D. J.; Zhou, H.-C. Construction of Ultrastable Porphyrin Zr Metal-Organic Frameworks through Linker Elimination. *J. Am. Chem. Soc.* **2013**, *135*, 17105. (c) Alezi, D.; Spanopoulos, I.; Tsangarakis, C.; Shkurenko, A.; Adil, K.; Belmabkhout, Y.; O'Keeffe, M.; Eddaoudi, M.; Trikalitis, P. N. Reticular Chemistry at Its Best: Directed Assembly of Hexagonal Building Units into the Awaited Metal-Organic Framework with the Intricate Polybenzene Topology, pbz-MOF. *J. Am. Chem. Soc.* **2016**, *138*, 12767. (d) Yuan, S.; Lu, W.; Chen, Y.-P.; Zhang, Q.; Liu, T.-F.; Feng, D.; Wang, X.; Qin, J.; Zhou, H.-C. Sequential Linker Installation: Precise Placement of Functional Groups in Multivariate Metal-Organic Frameworks. *J. Am. Chem. Soc.* **2015**, *137*, 3177. (e) Furukawa, H.; Gandara, F.; Zhang, Y.-B.; Jiang, J.; Queen, W. L.; Hudson, M. R.; Yaghi, O. M. Water Adsorption in Porous Metal-Organic Frameworks and Related Materials. *J. Am. Chem. Soc.* **2014**, *136*, 4369. (f) Morris, W.; Volosskiy, B.; Demir, S.; Gandara, F.; McGrier, P.-L.; Furukawa, H.; Cascio, D.; Stoddart, J. F.; Yaghi, O. M. Synthesis, Structure, and Metalation of Two New Highly Porous Zirconium Metal-Organic Frameworks. *Inorg. Chem.* **2012**, *51*, 6443.

DOI: 10.1021/jacs.9b07700
J. Am. Chem. Soc. 2019, 141, 14443−14450

(29) Jiang, H.-L.; Feng, D.; Wang, K.; Gu, Z.-Y.; Wei, Z.; Chen, Y.-P.; Zhou, H.-C. An Exceptionally Stable, Porphyrinic Zr Metal-Organic Framework Exhibiting pH-Dependent Fluorescence. *J. Am. Chem. Soc.* **2013**, *135*, 13934.
(30) Deria, P.; Gómez-Gualdrón, D. A.; Hod, I.; Snurr, R. Q.; Hupp, J. T.; Farha, O. K. Framework-Topology-Dependent Catalytic Activity of Zirconium-Based (Porphinato)zinc(II) MOFs. *J. Am. Chem. Soc.* **2016**, *138*, 14449.
(31) Eschenbrenner-Lux, V.; Kumar, K.; Waldmann, H. The Asymmetric Hetero-Diels-Alder Reaction in the Syntheses of Biologically Relevant Compounds. *Angew. Chem., Int. Ed.* **2014**, *53*, 11146.
(32) Cavka, J. H.; Jakobsen, S.; Olsbye, U.; Guillou, N.; Lamberti, C.; Bordiga, S.; Lillerud, K. P. A New Zirconium Inorganic Building Brick Forming Metal Organic Frameworks with Exceptional Stability. *J. Am. Chem. Soc.* **2008**, *130*, 13850.
(33) Spek, A. L. Single-crystal structure validation with the program PLATON. *J. Appl. Crystallogr.* **2003**, *36*, 7.
(34) (a) Jia, J.; Lin, X.; Wilson, C.; Blake, A. J.; Champness, N. R.; Hubbersty, P.; Walker, G.; Cussen, E. J.; Schröder, M. Twelve-connected porous metal-organic frameworks with high H_2 adsorption. *Chem. Commun.* **2007**, 840. (b) Zhang, X.-M.; Zheng, Y.-Z.; Li, C.-R.; Zhang, W.-X.; Chen, X.-M. Unprecedented (3,9)-Connected $(4^2 \cdot 6)_3(4^6 \cdot 6^{21} \cdot 8^9)$ Net Constructed by Trinuclear Mixed-Valence Cobalt Clusters. *Cryst. Growth Des.* **2007**, *7*, 980. (c) Volkringer, C.; Popov, D.; Loiseau, T.; Guillou, N.; Férey, G.; Haouas, M.; Taulelle, F.; Mellot-Draznieks, C.; Burghammer, M.; Riekel, C. A microdiffraction set-up for nanoporous metal-organic-framework-type solids. *Nat. Mater.* **2007**, *6*, 760. (d) Volkringer, C.; Mihalcea, I.; Vigier, J.-F.; Beaurain, A.; Visseaux, M.; Loiseau, T. Metal-Organic-Framework-Type 1D-Channel Open Network of a Tetravalent Uranium Trimesate. *Inorg. Chem.* **2011**, *50*, 11865. (e) Xia, Y.-P.; Wang, C.-X.; Feng, R.; Li, K.; Chang, Z.; Bu, X.-H. A novel double-walled Cd(II) metal-organic framework as highly selective luminescent sensor for $Cr_2O_7^{2-}$ anion. *Polyhedron* **2018**, *153*, 110. (f) He, T.; Zhang, Y.-Z.; Kong, X.-J.; Yu, J.; Lv, X.-L.; Wu, Y.; Guo, Z.-J.; Li, J.-R. Zr(IV)-Based Metal-Organic Framework with T-Shaped Ligand: Unique Structure, High Stability, Selective Detection, and Rapid Adsorption of $Cr_2O_7^{2-}$ in Water. *ACS Appl. Mater. Interfaces* **2018**, *10*, 16650. (g) Wang, Y.; Feng, L.; Fan, W.; Wang, K.-Y.; Wang, X.; Wang, X.; Zhang, K.; Zhang, X.; Dai, F.; Sun, D.; Zhou, H.-C. Topology Exploration in Highly Connected Rare-Earth Metal-Organic Frameworks via Continuous Hindrance Control. *J. Am. Chem. Soc.* **2019**, *141*, 6967.
(35) Zou, X.; Yang, L.; Liu, X.; Sun, H.; Lu, H. Silver Tetrafluoroborate-Catalyzed Oxa-Diels-Alder Reaction Between Electrically Neutral Dienes and Aldehydes. *Adv. Synth. Catal.* **2015**, *357*, 3040.
(36) Fujiwara, K.; Kurahashi, T.; Matsubara, S. Cationic Iron(III) Porphyrin-Catalyzed [4 + 2] Cycloaddition of Unactivated Aldehydes with Simple Dienes. *J. Am. Chem. Soc.* **2012**, *134*, 5512.
(37) Johnson, J. A.; Petersen, B. M.; Kormos, A.; Echeverría, E.; Chen, Y.-S.; Zhang, J. A New Approach to Non-Coordinating Anions: Lewis Acid Enhancement of Porphyrin Metal Centers in a Zwitterionic Metal-Organic Framework. *J. Am. Chem. Soc.* **2016**, *138*, 10293.
(38) Feng, D.; Gu, Z.-Y.; Chen, Y.-P.; Park, J.; Wei, Z.; Sun, Y.; Bosch, M.; Yuan, S.; Zhou, H.-C. A Highly Stable Porphyrinic Zirconium Metal-Organic Framework with shp-a Topology. *J. Am. Chem. Soc.* **2014**, *136*, 17714.

DOI: 10.1021/jacs.9b07700
J. Am. Chem. Soc. 2019, 141, 14443−14450